HHS Public Access

Author manuscript

Arthritis Rheumatol. Author manuscript; available in PMC 2022 February 25.

Published in final edited form as:

Arthritis Rheumatol. 2020 September ; 72(9): 1447–1455. doi:10.1002/art.41311.

Altered Lymphatic Vessel Anatomy and Markedly Diminished Lymph Clearance in Affected Hands of Patients With Active Rheumatoid Arthritis

Richard D. Bell[1], **Homaira Rahimi**[2], **H. Mark Kenney**[1], **Alicia A. Lieberman**[3], **Ronald W. Wood**[1], **Edward M. Schwarz**[1], **Christopher T. Ritchlin**[3]

[1]Center for Musculoskeletal Research, University of Rochester Medical Center, Rochester NY

[2]Deparment of Pediatrics, University of Rochester Medical Center, Rochester NY

[3]Department of Medicine, University of Rochester Medical Center, Rochester NY

Abstract

Objective: Assess differences in lymphatic function of RA hands with active synovitis versus healthy controls (Ctl) via near infrared-indocyanine green (NIR-ICG) imaging.

Methods: NIR imaging of 13 Ctl and 8 RA subjects with active disease (DAS28 > 4.4) was performed following web space injection of 0.1ml of 100μM ICG. Percent ICG retention from the web spaces was determined via NIR imaging at baseline and 7±1 day after the initial injections; image analysis provided contraction frequency. ICG^+ LV length and branching architecture.

Results: Retention of ICG in RA hands increased compared to Ctl (84±28% vs. 53±19% respectively; $p<0.01$). The average contraction frequency in ICG^+ LV between Ctl and RA subjects (0.51±0.35 vs 0.53±0.39 contractions/min) did not differ. Total ICG^+ LV length in RA hands was reduced (58.3±15.0 vs. 71.4±16.1cm; $p<0.001$), concomitant with a decrease in the number ICG^+ basilic-LVs vs. Ctl ($p<0.05$).

Conclusions: Lymphatic drainage in the hands of RA patients with active disease was reduced compared to controls. This reduction was associated with less total length of ICG^+ LVs on the dorsal surface of the hands, which continued to contract at a similar rate to controls. These findings provide a plausible mechanism for exacerbation of synovitis and joint damage. Specifically, the accumulation and retention of inflammatory cells and catabolic factors in RA joints due to impaired efferent lymphatic flow. NIR-ICG imaging of RA hands is feasible and warrants formal investigation as a primary outcome measure of arthritis disease severity and/or persistence in future clinical trials.

INTRODUCTION

Rheumatoid Arthritis (RA) is a debilitating progressive immune-mediated inflammatory joint disease that can lead to chronic pain and functional impairment [1]. A major challenge for both patients and practitioners is the propensity of the disease to flare, and the relative refractory nature of persistent disease despite aggressive therapy [1]. New insights into the etiopathogenesis of RA are needed to identify new targets and improve treatment response. One area of interest receiving increased attention in RA is lymphatics pathology and

dysfunction based on preclinical arthritis models, where the lymphatic system is strongly implicated in the onset of synovitis and disease progression [2, 3].

The lymphatic system provides homeostatic turnover of interstitial fluid and trafficking of immune cells to the closest lymph node [4, 5]. Multiple studies in murine RA models demonstrated dramatic changes in both lymphatic vessel (LV) contractions and the joint draining lymph node (LN) volume with disease progression [6–17]. During the early and middle phases of musculoskeletal inflammation, the joint draining LN undergoes a rapid increase in volume several fold greater than unaffected LNs. Following this initial expansion, LN volume decreases, and this change is accompanied by a concomitant cessation of LV contractions. The loss of LN volume and LV contractility coincides with end stage disease, leading to the hypothesis that altered lymphatic function promotes and sustains synovitis and may serve as a biomarker to assess the activity and reversibility of chronic joint inflammation [2].

Imaging studies of lymphadenopathy in RA patients report significant alterations in the size and morphology of draining LNs. In a small cohort of flaring RA subjects, contrast enhanced MR imaging of draining LNs displayed a reduction of LN volume after treatment [18]. Manzo and colleagues used power Doppler ultrasound (PDUS) imaging of the axillary LNs in RA subjects with active hand disease to demonstrate hypertrophy of the node cortex without clinical lymphadenopathy along with a strong PDUS signal in the cortical and hilar regions [19]. Patients refractory to disease modifying anti-rheumatic drugs (DMARDs) displayed a significant increase in LN volume and PDUS signal compared to healthy controls24 weeks after the initiation of anti-TNF therapy and these LN characteristics were all decreased [20]. A retrospective chart review of 78 patients with RA who underwent a chest CT found that simple disease activity index (SDAI) scores were significantly higher in patients with mediastinal and axillary LNs larger than 10 mm compared to patients with LNs less than 10 mm [21]. While these reports focused on the joint draining LNs, studies investigating generalized LV function in RA have not been reported.

Near infrared (NIR) imaging enables quantification of lymphatic function following the injection of a fluorescent tracer that is incorporated into the interstitial fluid [22]. In murine models of inflammatory arthritis, NIR imaging studies following subdermal injections of indocyanine green (ICG) clearly demonstrated abnormal LV function during arthritic progression [2, 3, 6–9]. Other investigators have applied this technology to characterize LV dysfunction in lymphedema [23, 24]. Thus, we set out to characterize lymphatic function and anatomy of the hand in RA subjects with active hand disease compared to healthy controls. We hypothesized that RA subjects with active joint disease would have impaired lymphatic function and altered lymphatic anatomy compared to healthy controls.

Materials and Methods

Human Participants and Study Design

This study was approved by the University of Rochester Institutional Review Board and is posted on ClinicalTrial.gov Identifier: NCT02680067. All subjects provided informed consent and were 18 years of age or older. RA subjects were recruited if they met the 2010

ACR criteria for RA [25] and currently (at the first visit) had at least 2 tender or swollen joints. Exclusion criteria were: other active systemic disorders or inflammatory conditions, known allergic sensitivity to iodine, and pregnancy. The demographics of our Ctl and RA cohorts are presented in Table 1. Clinical characteristics of the RA cohort are presented in Table 2. Two groups were developed from this cohort, a clearance group and an anatomy group. In the clearance group, subjects were injected with ICG and imaged (described below) at the baseline visit. The Ctl subjects were imaged every 7±1 days for 3 consecutive weeks while the RA subjects were imaged again only at day 7. In the anatomy group, both groups were asked to participate in 2–5 visits and they were injected with ICG at each visit to assess lymphatic function parameters.

Indocyanine Green Injections and Near Infrared Lymphatic Imaging

The web spaces of both hands were scrubbed with iodine solution and injected with 0.1ml of 100μM ICG on 1–5 separate occasions (dependent on the study group) using a 31-gauge needle. NIR-ICG images were obtained with a custom FDA approved system. NIR excitation was provided using a pair of regulated power sources (SOL-R: Fiberoptics Technology Incorporated, Pomfret CT, Part Number FTIII16797) each with a tungsten halogen EKE-ER MR16 bulb (Illumination Technologies Inc., Part Number 9596ER). This bulb incorporates a nondichroic parabolic reflector that enhances NIR output, sending all light forward to a bandpass excitation filter centered at 769 nm with a width of 41 nm (Semrock Inc., Rochester NY. 769/41 nm BrightLine® single-band bandpass filter Part Number: FF01–769/41–25) that restricts the range of wavelengths emitted into a fiber optic light conduit (Fiberoptics Technology Incorporated Fiber optic light line, 6” Part FTISL16854–6; Volpi Manufacturing, Auburn, NY, Fiber Optic LightLine 5”, Part No. 42050.036) that each illuminate an elliptical field of interest. The illumination intensity and field homogeneity has been professionally evaluated. An excitation intensity limit of 1.8 mW cm^{-2} was adopted so as not to exceed the FDA mandated threshold. A Thorlabs USB power meter (PM16–121) was placed in the field to monitor delivered intensity.

Fluorescent excitation was captured with a KITE EMCCD camera (KI247-CL, Raptor Photonics), fitted with a Zeiss ZF-IR lens and a high pass 805 nm Semrock filter (Semrock BLP01–785R-25) immediately in front of the sensor. Image acquisition was performed by a custom LabVIEW application (National Instruments Vision Acquisition Software). Camera exposure duration (500ms), binning (none), and gain (400) were unchanged throughout the course of the experiment. The aperture was set at f/8 for clearance measurements and f/4–5.6 for contraction frequency and anatomy measurements. The camera and illumination system were attached to a stand with multi-axis adjustable mounts; a desktop computer and display were on a separate rolling cart. Still images were recorded as PNGs and stored for analysis.

To measure clearance of ICG from the web spaces, the distance from the lip of the lens to the 3rd MCP was measured and set to 60 ± 1 cm, the illumination intensity was set to 950 ± 20 μW cm^{-2}, and the aperture was confirmed to be at f/8. Fixed size regions of interest (ROIs) were placed over each web space and apparent fluorescent intensity was measured during each clinic visit. The average of the 2nd, 3rd, and 4th webs space fluorescent intensity minus the background autofluorescence of the skin was used for statistical analysis.

In order to assess LV contraction frequency, 10-minute videos segments of the 2 frame per second (fps) continuous video of the study visit were recorded for each hand at all injection visits. First, we determined which LV bundle the vessels that cross the wrist contribute to, the cephalic or basilic. Lymphatic anatomy of the hands and forearm have been characterized previously and we used these data as references [26–29]. ROIs were placed over the LVs and NIR-ICG signal intensity was measured over time and boluses of dye flowing through the LVs, marked by peaks in signal intensity, were counted (by RDB and HMK) to generate contractions per minute similar to previous murine NIR methods [16]. Contractions were quantified as both the sum and the average of all contractions on the basilic or cephalic bundle.

Lymphatic hand anatomy was quantified by manually segmenting the LVs of the hand using Amira (FEI, ThermoFisher) with the help of the videos and max intensity images generated in ImageJ (by RBD and HMK). Any vessel that had ICG move through it during the 10-minute hand imaging session was segmented for analysis. A spatial graph was generated from this segmentation using the AutoSkeleton Amira feature and graph statistics were calculated by Amira. Total length is the sum of all the Euclidian distances between paired points framing a segment. To assess specific alterations in lymphatic anatomy, three readers (HR, HMK, and RDB) scored to consensus the number of basilic and cephalic LVs at the wrist, mid-hand, and adjacent to the injection sites per the scoring guidelines (Supplemental Document). To calculate interclass correlation coefficients (ICCs), a representative subsample (n=7 per group) was selected, blinded, and reanalyzed independently (without consensus scoring) for total LV length and LV counts by the same readers.

Statistical Analysis

All statistical analysis was performed in JMP Pro 13 (SAS, Durham NC),Prism (GraphPad, San Diego, CA) or R statistical package (3.6.1). Normality for all continuous outcomes was assessed via a Shapiro-Wilks test. A t-test, or a paired t-test was used for all normally distributed outcomes, while a Wilcoxon Rank test was used if normality was not found. Since an assessment of changes in lymphatic anatomy and function from web space injections over time (between visits) has never been performed, we assumed each study visit was an independent observation. ICCs were calculated with the *irr* library (0.84.1) in the R.

Results

RA subjects have significantly impaired clearance from the web spaces of their hands

Representative images of healthy controls at baseline and at the second visit demonstrated a large reduction in NIR-ICG signal intensity at the web spaces (Figure 1A, B, arrows). Strikingly, RA subjects show similar ICG fluorescent signal in the web spaces between the two visits (Figure 1C and D, arrows). When this NIR-ICG signal is quantified, RA subjects demonstrate a significantly higher retention of fluorescent signal from Day 0 to Day 7 compared to Ctl ($1.7\pm0.7\times10^4$ to $1.5\pm1.1\times10^4$ vs $2.0\pm0.6\times10^4$ to $1.1\pm0.5\times10^4$, $p<0.01$, Figure 1E). To understand the typical fluorescent half-life of ICG disappearance in

the web space, we measured the Ctl subjects for two additional weeks, or until the dye was undetectable, and determined the half-life to be 6.8 [3.4, 21.1] days (95% CI, Figure 1F).

Functional lymphatic anatomy is altered in RA subjects

To investigate if lymphatic anatomy (i.e. total number of LVs filled with ICG clearing the web spaces) was contributing to the deficiency in ICG clearance from the web spaces, we quantified the total length and number of ICG filled LVs. Interestingly, there is a significant r difference in the length and number of ICG filled LVs for Ctl and RA subjects (representative images Figure 2A and B, respectively), with a notable decrease in LVs overall in the RA subjects. When we quantified the total LV length, a significant decrease in RA subjects was noted compared to Ctls (58.3±15.0 cm vs 71.4±16.1 cm, respectively, $p<0.001$, Figure 2C). In order to identify if a reduction in specific LVs could explain this decrease in total LV length, we quantified LVs associated with the basilic and cephalic tracts at the wrist, mid-hand, and adjacent to the injection sites. Interestingly, significantly fewer basilic-associated LVs were counted at both the wrist and mid-hand in the RA subjects compared to Ctl (Figure 3D and E). No significant differences in cephalic-associated LVs at the wrist or mid-hand were found between RA subjects and Ctl (Figure 2F and G, respectively).

To validate the reliability of the quantification of LV length and counts, we chose a representative subsample (n=7 per group) was selected, blinded, and re-analyzed for total LV length and LV counts to calculate an ICC (Table 3). Total LV length was found to have the highest ICC at 0.95, indicating total length is the most reliable independent outcome. LV counts of the cephalic web space, cephalic mid-hand, and basilic wrist demonstrated moderate reliability (ICC:0.7–0.9). However, the basilic webspace, basilic mid-hand, and cephalic wrist counts all had poor reliability (ICC: 0.5–0.7), suggesting that these analysis methods require more refined scoring guidelines to remove any ambiguity in the process. Overall, however, we have confidence in the total LV length assessment, and the grading to consensus for the number of specific LVs, as reliable outcome measures of LV anatomy.

RA subjects do not have significant changes in contractility of their ICG filled LVs.

The difference in web space ICG clearance was not associated with alterations in LV contractility (Figure 3). LV contractions in the hand is a novel outcome measure, and because there are not consistent numbers of LVs associated with the cephalic and basilic lymphatic tracts between subjects (see Figure 1A vs Figure 2A), we chose to quantify the data via two different methods: 1) the average contraction frequency for all LVs on either the basilic or cephalic side (typically either 2 or 3 vessels each side) and 2) the sum of the total number of contractions in the LVs on either the basilic or cephalic side. Both methods considered the basilic and cephalic sides to be independent outcome measures. However, regardless of the methods used to quantify the data, no differences were observed between Ctl and RA subjects in basilic or cephalic LV contraction frequency (Figure 3A–D).

DISCUSSION

Herein, we provide the first characterization of lymphatic function and vascular anatomy of the hands of healthy controls and RA patients using NIR-ICG imaging. We find that RA subjects have reduced lymphatic clearance and a lower number of fluorescent LVs in the hands compared to control subjects. These findings provide support for the concept that these lymphatic alterations work synergistically or in parallel to block egress of inflammatory cells and molecules from rheumatoid joints fostering the development of synovitis and disease progression.

The effect of inflammation on lymphatic vasculature is well established and may provide insight into the contribution of lymphatic dysfunction in RA pathogenesis [30]. In particular, TNFα and IFNγ decrease lymphatic endothelial cell proliferation, capillary formation, and barrier integrity in vitro [31]. Additionally, inhibiting TNFα in murine arthritis models and RA is associated with increased lymphangiogenesis [32]. Injection of the lymphangiogenic growth factor VEGF-C into the ankles of TNF-transgenic mice, a chronic model of RA, promoted lymphatic capillary formation followed by enhanced lymphatic drainage alterations, and was associated with a significant improvement in joint inflammation and damage [33]. Conversely, blocking VEGFR3, the cognate receptor for VEGF-C, increased arthritis severity and decreased lymphatic function in TNF-transgenic mice [34]. The finding of a significant reduction in hand LVs in RA subjects is consistent with these data, suggesting that chronic exposure to inflammatory stimuli (e.g. TNF) may decrease the total number of functional LVs (i.e. LVs able to fill with ICG). On the other hand, lymphangiogenesis, a primary response during inflammation [4] is directly induced by TNF along with other factors [35]. This apparent mechanistic paradox likely arises due to complex interactions dependent on the concentration and duration of these inflammatory stimuli as well as other mediators produced in the RA joint. Surprisingly, we did not expect LV contraction to be maintained in RA patients with diminished lymphatic clearance. A potential explanation is that there are fewer functional vessels to carry the lymph fluid despite maintenance of contraction frequency resulting in diminished clearance. Alternatively, there might be a change in the amplitude of the LV contraction that cannot be measured with our current methods.

Inflammatory molecules also can directly influence lymphatic function. For example, LV contraction frequency is depressed when exogenous TNFα or IL-1β is injected into WT mouse hindlimbs [36]. When L-NIL, an inducible nitric oxide (NO) inhibitor, is delivered to these mice, the LV contraction frequency recovers to homeostatic levels [36]. The efficacy of blocking NO was examined in a study that trialed a NO inhibitor (GW274150) as a novel therapeutic option for patients with early RA. After 28 days of therapy, the NO inhibitor did not significantly decrease DAS28 scores or synovitis scoring via ultrasound compared to placebo, while prednisone significantly reduced both outcomes [37]. The limited effectiveness of NO inhibitors in the treatment of RA may be due to the various roles NO plays in the bone and lymphatic microenvironments [16, 38], along with our finding that RA patients do not have LV contraction deficits (Figure 3). Our results suggest that LV contraction frequency may not significantly contribute to lymphatic clearance of the

web spaces, and thus therapeutic intervention targeting LV contraction frequency may not be efficacious in treating RA.

One significant limitation of this study is that detailed mapping of the specific lymphatic vasculature clearing the joints of the hand is not available. For the purposes of this study, we assumed that web space lymphatic clearance accurately estimates the lymphatic drainage of the joint as assessed by NIR-ICG imaging. Cadaver studies that we (unpublished data) and others [29, 39] performed investigating superficial LVs from various subdermal injection sites in the hands detailed LVs running directly adjacent to the MCPs that likely contribute to drainage of the joint. No studies provide a detailed analysis of lymphatic vasculature draining the joint; addressing this gap is an active area of research.

Another limitation is that the molecular interactions of intradermal ICG, in patients with inflammatory disorders, are unknown. These interactions may alter ICG clearance from the web spaces independently of lymphatic function. Notably, ICG requires a substrate to interact with in order to become fluorescent [40], and exhibits a high affinity for lipoproteins [41, 42]. While RA patients tend to have relatively lower serum concentrations of total lipoprotein [43], most of our RA cohort has a history of hypertension or hyperlipidemia (Table 2). In our study, once the free ICG was injected into the web spaces of the hands in the RA subjects, the ICG may have bound the more abundant lipoproteins resulting in a lower clearance of free ICG (within the first 5 mins) compared to the healthy controls.

In this observational study, we provide initial insights into changes in lymphatic function and anatomy in RA patients with active disease. Observational cohorts with varying degrees of RA activity and damage coupled with data from large-scale clinical trials will further elucidate the lymphatic mechanisms in RA. Specifically, studies that control for disease duration, disease activity level, and treatment history will be important to show the temporal and therapeutic effects on lymphatic dysfunction described in mice [2]. Most importantly, our findings underscore the potential contribution of the lymphatic system to the initiation and persistence of synovial inflammation and highlight, the potential utility of NIR-ICG imaging as a biomarker of disease. Additional investigations into the mechanisms that promote or restrict lymphatic flow from synovial tissue have the potential to reveal new targets and improve clinical outcomes for RA patients.

Supplementary Material

Refer to Web version on PubMed Central for supplementary material.

ACKNOWLEDGEMENTS:

This research was supported by NIAMS grants (T32 AR053459, K08 AR067885, R01 AR056702 & P30 AR069655)

References

1. Firestein GS, The disease formerly known as rheumatoid arthritis. Arthritis Res Ther, 2014. 16(3): p. 114. [PubMed: 25167330]

2. Bouta EM, et al. , Targeting lymphatic function as a novel therapeutic intervention for rheumatoid arthritis. Nat Rev Rheumatol, 2018. 14(2): p. 94–106. [PubMed: 29323343]

3. Rahimi H, et al. , Lymphatic imaging to assess rheumatoid flare: mechanistic insights and biomarker potential. Arthritis Res Ther, 2016. 18: p. 194. [PubMed: 27586634]

4. Alitalo K, The lymphatic vasculature in disease. Nat Med, 2011. 17(11): p. 1371–80. [PubMed: 22064427]

5. Aspelund A, et al. , Lymphatic System in Cardiovascular Medicine. Circ Res, 2016. 118(3): p. 515–30. [PubMed: 26846644]

6. Bouta EM, et al. , Brief Report: Treatment of Tumor Necrosis Factor-Transgenic Mice With Anti-Tumor Necrosis Factor Restores Lymphatic Contractions, Repairs Lymphatic Vessels, and May Increase Monocyte/Macrophage Egress. Arthritis Rheumatol, 2017. 69(6): p. 1187–1193. [PubMed: 28118521]

7. Bouta EM, et al. , The role of the lymphatic system in inflammatory-erosive arthritis. Semin Cell Dev Biol, 2015. 38: p. 90–7. [PubMed: 25598390]

8. Bouta EM, et al. , In vivo quantification of lymph viscosity and pressure in lymphatic vessels and draining lymph nodes of arthritic joints in mice. J Physiol, 2014. 592(6): p. 1213–23. [PubMed: 24421350]

9. Li J, et al. , Efficacy of B cell depletion therapy for murine joint arthritis flare is associated with increased lymphatic flow. Arthritis Rheum, 2013. 65(1): p. 130–8. [PubMed: 23002006]

10. Bouta EM, et al. , Power Doppler ultrasound phenotyping of expanding versus collapsed popliteal lymph nodes in murine inflammatory arthritis. PLoS One, 2013. 8(9): p. e73766. [PubMed: 24040061]

11. Bouta EM, et al. , Measuring intranodal pressure and lymph viscosity to elucidate mechanisms of arthritic flare and therapeutic outcomes. Ann N Y Acad Sci, 2011. 1240: p. 47–52. [PubMed: 22172039]

12. Zhou Q, et al. , Near-infrared lymphatic imaging demonstrates the dynamics of lymph flow and lymphangiogenesis during the acute versus chronic phases of arthritis in mice. Arthritis Rheum, 2010. 62(7): p. 1881–9. [PubMed: 20309866]

13. Proulx ST, et al. , MRI and quantification of draining lymph node function in inflammatory arthritis. Ann N Y Acad Sci, 2007. 1117: p. 106–23. [PubMed: 17646265]

14. Proulx ST, et al. , Longitudinal assessment of synovial, lymph node, and bone volumes in inflammatory arthritis in mice by in vivo magnetic resonance imaging and microfocal computed tomography. Arthritis Rheum, 2007. 56(12): p. 4024–37. [PubMed: 18050199]

15. Liang Q, et al. , Lymphatic endothelial cells efferent to inflamed joints produce iNOS and inhibit lymphatic vessel contraction and drainage in TNF-induced arthritis in mice. Arthritis Res Ther, 2016. 18: p. 62. [PubMed: 26970913]

16. Bell RD, et al. , iNOS dependent and independent phases of lymph node expansion in mice with TNF-induced inflammatory-erosive arthritis. Arthritis Res Ther, 2019. 21(1): p. 240. [PubMed: 31727153]

17. Bell RD, et al. , Selective Sexual Dimorphisms in Musculoskeletal and Cardiopulmonary Pathologic Manifestations and Mortality Incidence in the Tumor Necrosis Factor-Transgenic Mouse Model of Rheumatoid Arthritis. Arthritis Rheumatol, 2019. 71(9): p. 1512–1523. [PubMed: 30969024]

18. Rahimi H, et al. , Relationship Between Lymph Node Volume and Pain Following Certolizumab Therapy for Rheumatoid Arthritis Flare: A Pilot Study. Clin Med Insights Arthritis Musculoskelet Disord, 2016. 9: p. 203–208. [PubMed: 28008295]

19. Manzo A, et al. , Subclinical remodelling of draining lymph node structure in early and established rheumatoid arthritis assessed by power Doppler ultrasonography. Rheumatology (Oxford), 2011. 50(8): p. 1395–400. [PubMed: 21378108]

20. Manzo A, et al. , Power Doppler ultrasonographic assessment of the joint-draining lymph node complex in rheumatoid arthritis: a prospective, proof-of-concept study on treatment with tumor necrosis factor inhibitors. Arthritis Res Ther, 2016. 18(1): p. 242. [PubMed: 27770827]

21. Okabe Y, et al. , Mediastinal and axillar lymphadenopathy in patients with rheumatoid arthritis: prevalence and clinical significance. Clin Imaging, 2019. 55: p. 140–143. [PubMed: 30818164]

22. Rasmussen JC, et al. , Lymphatic imaging in humans with near-infrared fluorescence. Curr Opin Biotechnol, 2009. 20(1): p. 74–82. [PubMed: 19233639]
23. Aldrich MB, et al. , Lymphatic abnormalities in the normal contralateral arms of subjects with breast cancer-related lymphedema as assessed by near-infrared fluorescent imaging. Biomed Opt Express, 2012. 3(6): p. 1256–65. [PubMed: 22741072]
24. O'Donnell TF Jr., Rasmussen JC, and Sevick-Muraca EM, New diagnostic modalities in the evaluation of lymphedema. J Vasc Surg Venous Lymphat Disord, 2017. 5(2): p. 261–273. [PubMed: 28214496]
25. Aletaha D, et al. , 2010 Rheumatoid arthritis classification criteria: an American College of Rheumatology/European League Against Rheumatism collaborative initiative. Arthritis Rheum, 2010. 62(9): p. 2569–81. [PubMed: 20872595]
26. Suami H, Lymphosome concept: Anatomical study of the lymphatic system. J Surg Oncol, 2017. 115(1): p. 13–17. [PubMed: 27334241]
27. Suami H, et al. , Superficial lymphatic system of the upper torso: preliminary radiographic results in human cadavers. Plast Reconstr Surg, 2008. 121(4): p. 1231–9. [PubMed: 18349641]
28. Suami H and Scaglioni MF, Anatomy of the Lymphatic System and the Lymphosome Concept with Reference to Lymphedema. Semin Plast Surg, 2018. 32(1): p. 5–11. [PubMed: 29636647]
29. Suami H, Taylor GI, and Pan WR, The lymphatic territories of the upper limb: anatomical study and clinical implications. Plast Reconstr Surg, 2007. 119(6): p. 1813–22. [PubMed: 17440362]
30. Schwager S and Detmar M, Inflammation and Lymphatic Function. Front Immunol, 2019. 10: p. 308. [PubMed: 30863410]
31. Chaitanya GV, et al. , Differential cytokine responses in human and mouse lymphatic endothelial cells to cytokines in vitro. Lymphat Res Biol, 2010. 8(3): p. 155–64. [PubMed: 20863268]
32. Polzer K, et al. , Tumour necrosis factor blockade increases lymphangiogenesis in murine and human arthritic joints. Ann Rheum Dis, 2008. 67(11): p. 1610–6. [PubMed: 18174217]
33. Zhou Q, et al. , Vascular endothelial growth factor C attenuates joint damage in chronic inflammatory arthritis by accelerating local lymphatic drainage in mice. Arthritis Rheum, 2011. 63(8): p. 2318–28. [PubMed: 21538325]
34. Guo R, et al. , Inhibition of lymphangiogenesis and lymphatic drainage via vascular endothelial growth factor receptor 3 blockade increases the severity of inflammation in a mouse model of chronic inflammatory arthritis. Arthritis Rheum, 2009. 60(9): p. 2666–76. [PubMed: 19714652]
35. Ji H, et al. , TNFR1 mediates TNF-alpha-induced tumour lymphangiogenesis and metastasis by modulating VEGF-C-VEGFR3 signalling. Nat Commun, 2014. 5: p. 4944. [PubMed: 25229256]
36. Aldrich MB and Sevick-Muraca EM, Cytokines are systemic effectors of lymphatic function in acute inflammation. Cytokine, 2013. 64(1): p. 362–9. [PubMed: 23764549]
37. Seymour M, et al. , Ultrasonographic measures of synovitis in an early phase clinical trial: a double-blind, randomised, placebo and comparator controlled phase IIa trial of GW274150 (a selective inducible nitric oxide synthase inhibitor) in rheumatoid arthritis. Clin Exp Rheumatol, 2012. 30(2): p. 254–61. [PubMed: 22409880]
38. Zheng H, et al. , RANKL stimulates inducible nitric-oxide synthase expression and nitric oxide production in developing osteoclasts. An autocrine negative feedback mechanism triggered by RANKL-induced interferon-beta via NF-kappaB that restrains osteoclastogenesis and bone resorption. J Biol Chem, 2006. 281(23): p. 15809–20. [PubMed: 16613848]
39. Suami H, Pan WR, and Taylor GI, Changes in the lymph structure of the upper limb after axillary dissection: radiographic and anatomical study in a human cadaver. Plast Reconstr Surg, 2007. 120(4): p. 982–91. [PubMed: 17805128]
40. Kraft JC and Ho RJ, Interactions of indocyanine green and lipid in enhancing near-infrared fluorescence properties: the basis for near-infrared imaging in vivo. Biochemistry, 2014. 53(8): p. 1275–83. [PubMed: 24512123]
41. Yoneya S, et al. , Binding properties of indocyanine green in human blood. Invest Ophthalmol Vis Sci, 1998. 39(7): p. 1286–90. [PubMed: 9620093]
42. Ott P, Hepatic elimination of indocyanine green with special reference to distribution kinetics and the influence of plasma protein binding. Pharmacol Toxicol, 1998. 83 Suppl 2: p. 1–48.

43. Liao KP, et al. , Lipid and lipoprotein levels and trend in rheumatoid arthritis compared to the general population. Arthritis Care Res (Hoboken), 2013. 65(12): p. 2046–50. [PubMed: 23925980]

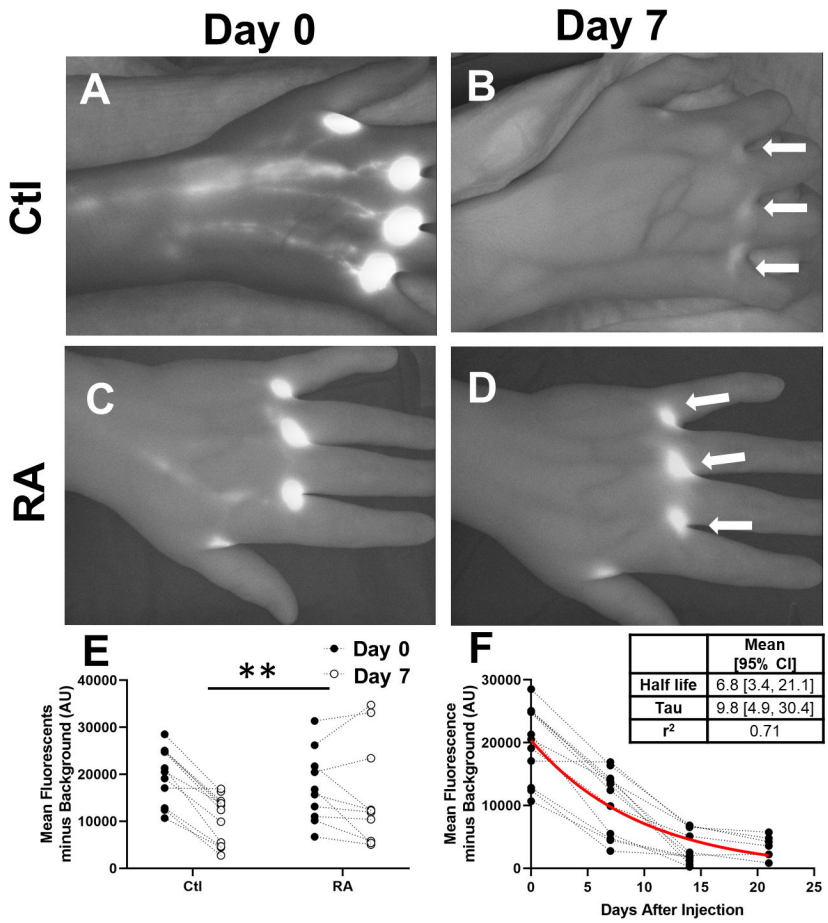

Figure 1. Impaired Lymphatic Clearance of ICG from the Hand in RA Subjects.

ICG intensity was measured in left and right hands of 6 control (Ctl, n=12) and 5 RA subjects (n=10) after injection at the initial visit and before new injections at the second visit 7 ± 1 days later (2nd Visit). Representative NIR images of a control subject at baseline (**A**) and at the second visit (**B**) show considerable clearance of the ICG at the injection sites (White Arrows), while in an RA subject (**C**, **D**) did not clear the ICG. When this was compared to RA subjects at visit 1 and visit 2, RA subjects had significantly less clearance (**E**, Repeated Measures ANOVA, **p<0.01). The cohort of control subjects underwent sequential imaging every 7 ± 1 days without further injections to determine one phase decay half-life of 6.8 [3.4, 21.1] days (Mean [95% CI], Best Fit Line in Red, Inset Table, **F**).

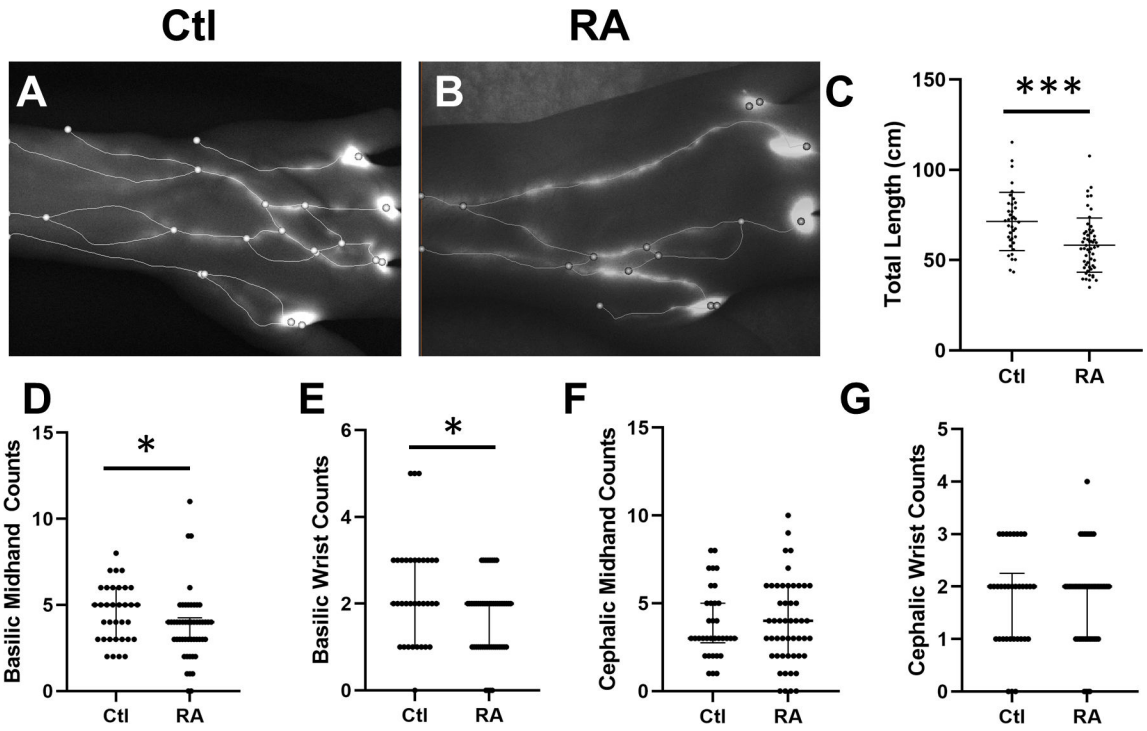

Figure 2. RA subjects have significantly fewer basilic associated web space clearing lymphatic vessels in their hands compared to healthy controls.

Representative stills of Ctl (**A**) and RA (**B**) hands with overlaid spatial graphs show significant variation between the two. Accordingly, RA subjects have significantly less total graph length (**C**, t-test, M±SD, **p<0.01). To investigate local differences, we manually scored to consensus the number of vessels at the wrist and mid hand. Interestingly, we found significantly fewer basilic associated vessels (**D** and **E**) while there was no change in cephalic sided vessels (**F** and **G**, Median and IQR, *p<0.05).

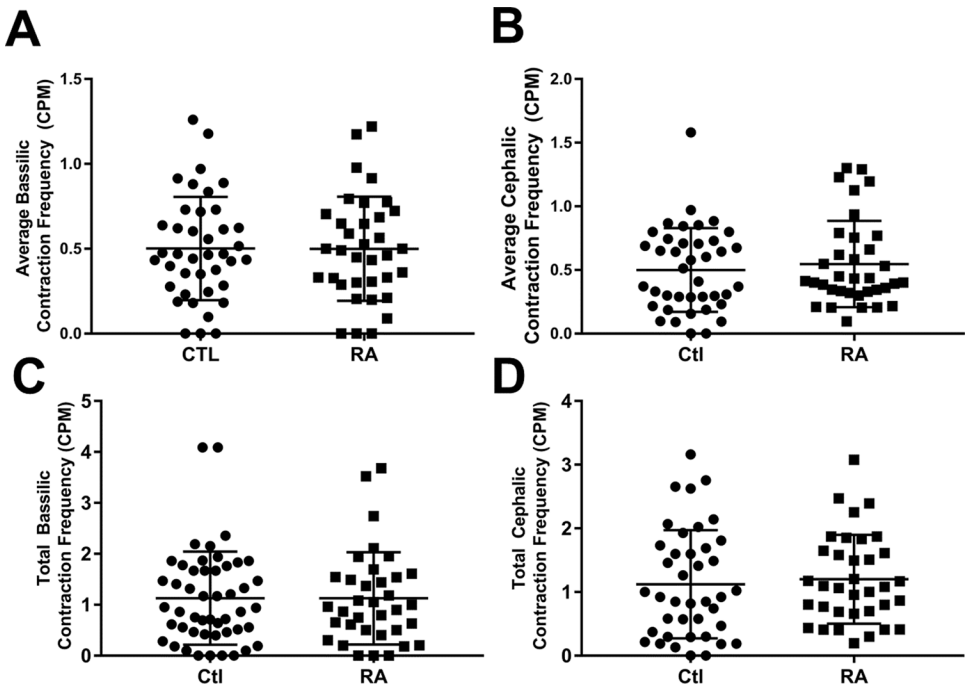

Figure 3. Lymphatic contraction frequency is not different between healthy controls and RA subjects.

Lymphatic contraction frequency was calculated via ROI analysis of 10 minutes observing the dorsal aspect of the hand. An ROI was placed over the basilic and cephalic associated vessels at the wrist. These data for each vessel were either averaged or summed to generate average basilic (A) and cephalic (B) contraction frequency; or total basilic (C) and cephalic (D) contraction frequency. There were no statistical differences between the groups for any of these outcomes.

Table 1.

Participant Demographics.

	Female (Total), %	Age (Yrs, M ± SD)	Race (African American : Asian : Caucasian)	BMI (M ± SD)	Grip Strength (kg)
Ctl	7(13), 54%	49.1 ± 14.3	2 : 1 : 10	29.8 ± 5.4	40 ± 10 ***
RA	8(8), 100%	55.8 ± 12.4	2:0:6	34 ± 8.7	22 ± 19 ***

Statistical significance indicated between Ctl and RA

*** p<0.001.

Table 2.

RA cohort description.

Current Joint Involvement	Duration of Symptoms	Serology	Acute-Phase Reactants	DAS	Current Relevant Comorbidities	Current Relevant Medications
Bilateral Wrists	3 weeks	CCP =17.5	CRP:148	4.44	N/A	N/A
Bilateral MCPs and PIPs	6 weeks	RF: 160, CCP: >250	ESR= 36	5.6	Hypertension	methotrexate
Right MCP's, PIP's and wrist	6 weeks	CCP: 122	ESR=69; CRP= 25	4.45	Hypertension, Hypothyroid	methotrexate
Bilateral MCPs and PIPs	3 months	RF:289, CCP: >300	CRP:1.19, ESR:33	4.51	Hypertension	N/A
Bilateral Wrists, bilateral 2nd and 3rd PIP	1 year	CCP:>250	ESR: 115, CRP:15	5.63	Hypertension, Pulmonary Fibrosis	méthylprednisolone, meloxicam, hydroxychloroquine, Adalimumab, mycophenolic acid (for Fibrotic ILD)
Right wrist, MCP's, DIP'S	2 years	CCP: 144, RF: 136,	CRP 1.5	5.15	COPD, Hyperlipidemia	methotrexate
Bilateral all MCPs, bilateral wrists	30 years	CCP:35	ESR: 69, CRP:35	5.05	N/A	etanercept
All MCPs, Bilateral Wrist, Bilateral Elbow	50 years	RF+	ESR:56, CRP:6.7	4.76	Hypertension	leflunomide, tofacitinib,, prednisone, hydroxychloroquine

CCP = Cyclic Citrullinated Peptide; RF=Rheumatoid Factor; MCP = Metacarpophalangeal joint; PIP = Proximal interphalangeal joint; CRP = C-reactive protein; ESR = Erythroid sedimentation rate, DAS = Disease activity score, ILD = Interstitial lung disease

Table 3.

Interclass correlation coefficients for lymphatic vasculature anatomy grading.

	ICC
Total Length	0.95
Basilic Webspace	0.67
Basilic Mid Hand	0.54
Basilic Wrist	0.74
Cephalic Webspace	0.90
Cephalic Mid Hand	0.71
Cephalic Wrist	0.64